p-ISSN 2089 – 0133 e-ISSN 2477-6416
URL: https://jurnal.uns.ac.id/ijap/article/view/87564

DOI: https://doi.org/10.13057/ijap.v15i1.87564

ADSORPTION BEHAVIOR OF SUGARCANE BAGASSE-DERIVED ACTIVATED CARBON AS A COPPER REMOVAL

Nur Layli Amanah[1,2], Alsello Diveni Manuputty[1], Fadila Arum Ramadhani[1,2], Dita Floresyona[1], Eduardus Budi Nursanto[1], Haryo Satriya Oktaviano[1,3], Agung Nugroho*[1]

[1]Department of Chemical Engineering, Universitas Pertamina, Jakarta, Indonesia
[2]Department of Materials Science and Engineering, National Taiwan University of Science and Technology, Taipei, Taiwan
[3]Technology Innovation, PT. Pertamina (Persero), Jakarta, Indonesia
*agung.n@universitaspertamina.ac.id

Received 04-06-2024, Revised 18-09-2024, Accepted 27-02-2025,
Available Online 01-04-2025, Published Regularly April 2025

ABSTRACT

This study aims to remove Cu^{2+} as a heavy metal inside the sample solution implementation. Eliminating heavy metals through activated carbon utilizes sugarcane bagasse's high carbon content, which is rich in cellulose, lignin, and hemicellulose. There are various methods for eliminating metal content, including activation using Acid 0.1 M Hydrochloric Acid (HCl), Base 0.1 M Sodium Hydroxide (NaOH), and without using activation media. The method considers the different ion Cu^{2+} initial concentrations and contact times. Detailed initial concentrations of Cu^{2+} were conducted using $CuSO_4$ media for 2.5, 5, 10, and 15 ppm and 15, 30, 60, and 120 minutes for length of contact time. For the result, the transmittance of FTIR showed a primary functional group of Activated Carbon (AC) on SBAC-1, comprising O-H, C-O, and C=O. The Brunauer-Emmett-Teller (BET) analysis also shows the significant value reaching 458.607 m^2/g surface area's adsorption and had q_{max} = 8.13 mg/g, the highest adsorption capacity. The plot brings about the adsorption mechanism as physiochemical & multilayer adsorption, with a physisorption layer with percent removal of Cu^{2+} at 81.3% at 30 minutes optimum time and optimum initial concentration of 5 mg/L with 82.2 % absorption on SBAC-1. The determination of Freundlich as the isotherm model is the most suitable mechanism of absorption for all process variations and generates a R^2 value of 0.9731 for the SBAC-1 sample.

Keywords: Adsorption; Wastewater; Activated Carbon; Copper Ion; Sugarcane Bagasse

Cite this as: Amanah, N. L., Manuputty, A. D., Ramadhani, F. A., Floresyonaa, D., Nursanto, E. B., Oktaviano, H. S., & Nugroho, A. 2025. Adsorption Behavior of Sugarcane Bagasse-Derived Activated Carbon As A Copper Removal. *IJAP: Indonesian Journal of Applied Physics, 15*(1), 98-109. doi: https://doi.org/10.13057/ijap.v15i1.87564

INTRODUCTION

Nowadays, Indonesia's electroplating sector is seeing growth. Initially, it was limited to household scale, but as demand for plated components increased, it has grown into a large-scale business, particularly in the automotive and steel industries [1-3] However, it is essential to remember that the electroplating process produces waste, which can significantly impact the large industry[4]. The wastewater industry has various ways to treat effluents and remove heavy metals before releasing them into the environment. These methods include ion exchange, chemical separation, electro-flotation, and reverse osmosis [5]. Adsorption is

highly effective and cost-efficient in purifying wastewater from heavy metals. It is also a simple and environmentally friendly process that can be carried out using various adsorbents. Therefore, the adsorption method is one of the most hopeful approaches to managing industrial wastewater [6] . Activated carbon (AC) is highly effective at removing heavy metals from liquid effluents and is considered one of the best adsorbents. Activated carbon is widely prepared by various biomass such as mango peel [6], Coconut Shell [7], sawdust [8], bran/rice husk [9], etc. Besides the previous test, Zakir and co-workers reached the BET analysis of activated carbon at about 125.828 m^2/g and 142.435 m^2/g to measure the surface area and porous materials. They use candlenut husk as a raw material and acid activation by H_3PO_4 85% by volume ratio H_3PO_4/carbon mass of 6:1 with a 24-hour soak time [10].

Sugarcane is one of the popular plants in Indonesia. Sugarcane extract is usually used as a healthy, valuable drink for the human body. Besides that, sugarcane has also become a raw material for sugar manufacturing. Since sugarcane was being used, much waste was created and priceless. Bagasse waste is commonly used as a source of fuel for boilers and animal feed and as a raw material for fertilizer [11]. However, it can be transformed into activated carbon as an adsorbent to remove heavy metals in wastewater for safer disposal following government regulations regarding waste disposal. Despite its limited economic value, this process has potential benefits, enabling the absorption of Cu^{2+} in wastewater [12-13].

Based on previous research, Al Nadine et al. synthesized NiO-Carbon composite using sugarcane bagasse through hydrothermal impregnation with NaOH as an activator [14]. Their experiment found that the BET surface area of the pristine porous carbon is 57.81 m^2/g, which is beneficial for electrochemical properties. The small surface area was due to the impregnation of NiO in the carbon structure. We expect to increase the surface area without adding metal oxide and varying the process variable. In this work, activated carbon made from sugarcane bagasse was used in an adsorption investigation of Cu^{2+} metal ions that were dissolved in water and showed an increase in the BET value up to 458.607 m^2/g. Three alternative techniques were employed to activate the AC in Table 1 to understand better how the adsorption process works due to the extended contact duration and elevated activation concentration. The detailed adsorption process was then studied using several models, including the Freundlich and Langmuir isotherm. The research concentrated on the factors related to processing parameters and the variations in the activation process. Atomic Adsorption Spectroscopy (AAS) was used to examine the sample's solution and count the Cu^{2+} ions left behind after the adsorption procedure. Fourier transforms infrared (FTIR), and Brunauer–Emmett–Teller (BET) were utilized to determine the chemical functional groups' content and measure the surface area of characteristic materials' activated carbon.

METHOD

Material and Synthesis

Various materials were necessary to produce Sugarcane Bagasse Activated Carbon (SBAC). The adsorbent was made from sugarcane bagasse, and $CuSO_45H_2O$ crystals were used to provide Cu^{2+} ions as a model solution for the adsorbates. All solutions were made using distilled water. 0.1 M HCl served as the acid activator and 0.1 M NaOH was used as the base activator (Table 1). During the carbonization process, argon gas was utilized to maintain inert conditions. The yield obtained from this technique is written detail in Table 1, the yield is obtained from the fixed carbon content of the carbonized sugarcane bagasse

(g) compared to the total weight of other compounds in the initial weight of the sugarcane bagasse (g).

The first step in preparing Sugarcane Bagasse was to remove the water content by drying it at 100ºC for 24 hours. The dried bagasse was then ground to speed up the carbonization process. Lists three approaches used to activate and carbonize the adsorbent following Table 1. One of these methods involved a physical process of gradually heating the material at ten degrees Celsius per minute. Another method used chemical activation, where the adsorbent was soaked in 0.1 M NaOH and 0.1 M HCl aqueous solution for two hours. The carbonization of the sample was repeated in a tube furnace for one hour at a temperature of 900°C.

Table 1. The activation process variation and yield result for the preparation of AC.

No.	Name of Sample	Detailed Activation Process	Yield (%)
1	SBAC-1	Chemical (Immersed in NaOH 0.1 M, 2 h) – physical (900ºC, 1 h)	23.69
2	SBAC-2	Chemical (Immersed in HCl 0.1 M, 2 h) – physical (900ºC, 1 h)	40.31
3	SBAC-3	Physical (400ºC, 1 h)	30.86

Characterization

The characterization was separated into two specimens. The initial step in evaluating the activated carbon involved the utilization of Fourier Transform Infrared Spectroscopy (FTIR) typically from 4000 cm^{-1} to 400 cm^{-1} wavelength to get the functional groups desired in the material content. The physical characteristics of the AC were also established using the Brunauer-Emmett-Teller (BET) analysis method from Quantachrome Instrument Pertamina Research and Technology and Innovation. In addition, we measured the concentration of metal ions in our wastewater samples using Atomic Absorption Spectrophotometry (AAS), AAS-GFS Thermo Scientific iCE 3000 Series type from Badan Riset dan Inovasi Nasional (BRIN).

Batch Adsorption Experiment

$CuSO_4$ was used as the source of the model solution for wastewater by dissolving it in distilled water. The concentration of ion Cu^{2+} in the model simulation wastewater was 2.5, 5, 10, and 15 ppm for each variation of initial concentration, contact time (15, 30, 60, and 120 minutes), and activation; 60 mL of adsorbate was prepared. The samples are each placed in a shaker and subjected to agitation at 150 rpm for one hour under atmospheric conditions and room temperature. Following the reaction, a vacuum filtration system separated the adsorbent and effluent samples. The AAS examines the adsorbate/effluent sample to determine the final concentration of Cu^{2+} adsorbate. Then, the removal percentage of adsorption and maximum adsorption capacity will be evaluated.

Equations 1 and 2 enable the calculation of two key parameters: the amount of Cu^{2+} concentration the activated carbon (i.e., the adsorbent) can absorb per unit of initial Cu^{2+} concentration. Also, the highest capacity of the adsorbent can be achieved at a specific mass and volume.

$$\%Removal = \frac{C_o - C_e}{C_o} \times 100\% \quad (1)$$

$$q_e = \frac{C_o - C_e}{W} x\ V \quad (2)$$

Several variables must be considered to evaluate the $\%Removal$ of the batch adsorption process, including the Cu^{2+} ion's initial concentration in the solution (C_o) and the final concentration of these ions following the procedure (C_e). Additionally, we need to know the maximum adsorbent capacity (q_e) through the sample volume (V) and the mass of the adsorbent used (W).

Determination of Experimental Model

To achieve the most effective correlation for equilibrium curves, optimizing the adsorption system's design and understanding the mechanism responsible for the adsorption of Cu^{2+} ions in aqueous solutions is necessary [15]. We employs the Freundlich and Langmuir isotherms to model the adsorption behaviour, which general equations are presented in equation 3 and 4, respectively.

$$\frac{Ce}{Qe} = \frac{1}{(KbAs)} + \frac{Ce}{As} \quad (3)$$

$$\log Q_e = \log K_f + \left(\frac{1}{n}\right) \log C_e \quad (4)$$

These equation represents a linear form of the Langmuir (3) and Freundlich (4) adsorption isotherm, respectively. These describe the relationship between the equilibrium concentration of the adsorbate (C_e) and the amount of adsorbate adsorbed per unit mass of the adsorbent (Q_e). In this equation, C_e is the concentration of the adsorbate in solution at equilibrium, typically measured in mg/L. At the same time, Q_e represents the amount of adsorbate adsorbed per unit mass in mg/g. The K value, known as the Langmuir constant (K_b) and Freaundlich constant (K_f), reflects the strength of the interaction between the adsorbate and the adsorbent. A_s refers to the surface area of the adsorbent in m^2/g, and indicates the amount of available surface for adsorption

While the regression by Langmuir model can be determined through the equation:

$$\frac{1}{q_{max}} = slope \quad (5)$$

$$\frac{1}{q_{max} \times K_L} = Intercept \quad (6)$$

The parameter q_{max} represents the maximum adsorption capacity of the adsorbent or the amount of adsorbate that can be adsorbed when the surface is fully occupied. At the same time, K_L is the Langmuir constant that reflects the adsorption affinity

RESULTS AND DISCUSSION

Activation of Activated Carbon

After drying and grinding, the sugarcane bagasse is heated to 400°C for one hour to start the pre-carbonization process. Next, the pre-carbonized sample will be activated using the activation process as shown in Table 1. NaOH is used to remove the carbonate impurities in the activated carbon during activation on the SBAC-1. During the reaction with NaOH activation, Natrium carbonate formed, as shows the possibility of another chemical reaction included in Equations 7 and 8 [16-17]. Meanwhile, SBAC-2, the acid activation by HCl

functioned as a hygroscopic compound that would allow dehydration and decrease the moisture content of activated carbon [18]. For the chemical activation, an impregnation method was employed with a 150 rpm agitator speed for 60 minutes at room temperature. This step was undertaken to enhance the energy and promote an optimal reaction.

$$4NaOH_{(s)} + C_{(s)} \rightarrow 4Na_{(s)} + CO_{2(g)} + 2H_2O_{(g)} \quad (7)$$

$$6NaOH_{(s)} + C_{(s)} \rightarrow 2Na_{(s)} + 3H_{2(g)} + 2Na_2CO_{3(s)} \quad (8)$$

During the carbonization, volatile compounds inside bagasse sugarcane are burned to release gases, such as CO, CO_2, CH_4, and H_2 [19]. The constituent compounds of bagasse also decomposed at 180°C for hemicellulose, while cellulose deteriorated at 270 – 310°C, and the last decomposition will happen to lignin starting from 350°C [20]. Thus, the second carbonization (900°C) yields less activated carbon than the first (400°C) because the second carbonization does not produce any ash formation due to argon gas as the atmospheric gas while heating the tube furnace from 200°C [6]. Besides that, argon gas has a function to avoid the presence of oxygen and form ash when burned.

Characterization of Activated Carbon

The functional group on each sample, SBAC-1, and SBAC-2, has been compared with the blank group without chemical reaction, SBAC-3. Figure 1 shows three primary spectra within the wavelength magnitude between 4000-500 cm^{-1}. There is a notable disparity in the chemical activation between SBAC-1 and SBAC-2 compared to SBAC-3. The O-H stretching peak spectra appeared in SBAC-1 and SBAC-3 samples at 3200-2800 cm^{-1} and 3700-3200 cm^{-1}, whereas in that wavelength range, no single peak was visible in SBAC-2. The reason is made possible by the activation acid compounds used cannot attract carbonate compounds such as NaOH as base activation [21]. In addition, two crucial functional groups in AC were found at wavelengths 1070-1000 cm^{-1} and 1520-1490 cm^{-1}. The three SBAC samples exhibit peaks indicating C-O and C=O functional groups, as shown by the appropriate spectra. Especially for SBAC-2, the C-O bond has a smaller peak than the others, related to the acid-immersed compound used for the activation process. The HCl will cause dehydration reactions that aid in carbonization but do not contribute additional oxygen to the structure and lead to fewer C-O groups remaining, reflected as a small peak at 1070-1000 cm^{-1} [22].

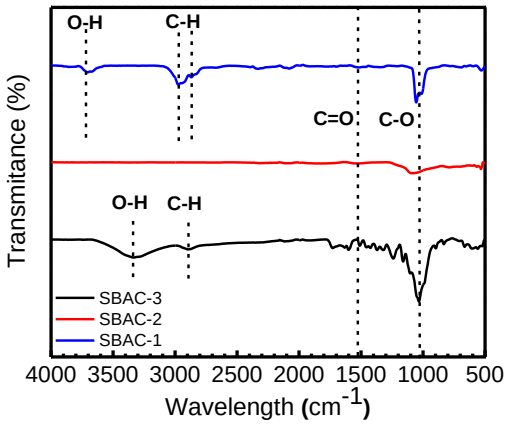

Figure 1. FTIR Spectrum of Activated Carbon

AC's surface area and adsorption capacity are comprehensively detailed in Table 2, as conducted by BET through difference activation. The most prominent surface area was occupied by SBAC-1, reaching 458.607 m^2/g, followed by SBAC-3 and SBAC-2, 25.711 m^2/g and 20.408 m^2/g sequentially. The adsorption capacity of the carbon surface is affected by the loss of volatile compounds and erosion, which leads to an increase in the activation surface area and the opening of its pores [23].

Certainty occurs in SBAC-2 activated carbon; the surface area obtained the lowest in comparison to the other samples, closely related to the presence of impurities contamination, which causes the closure of microspores on the surface of the adsorbent [24]. The surface area and adsorption capacity were determined through leading BET analysis linearity occurs in the SBAC-1 sample, which means the SBAC-2 led to a blockage on the surface of the micro-pores, thereby hindering the adsorbent's surface area [25]. That statement is supported by the low value of the volume absorbed by activated carbon, which is used to determine the surface area and porosity of the material. So, as the volume taken (V_T) during testing increases, the surface area and porosity will increase, which has been proven and can also be seen in Table 3 [26].

Table 2. Activated carbon's physical properties.

No.	Name of Sample	Activation	Surface Area (m^2/g)	Pore Volume (cm^3/g)	Pore size (nm)
1.	SBAC-1	Base	458.607	0.171	3.461
2.	SBAC-2	Acid	20.408	0.027	3.199
3.	SBAC-3	Physical	25.711	0.028	3.445

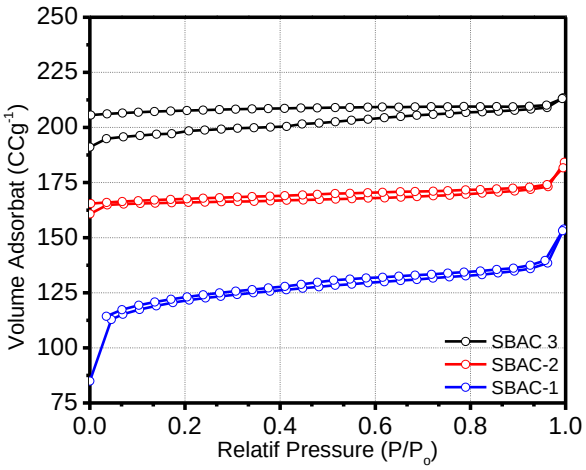

Figure 2. Isotherm's graph of adsorption-desorption of all synthesized samples.

Figure 2 in the BET study shows the linearization of isotherm adsorption-desorption by N_2 gas. At low relative pressure (P/P_o), the available adsorbate volume was initially low, then rose drastically for a moment, got flattens to the higher relative pressures (P/P_o= 0.9), and increased the volume of adsorbates with a high level. This type of graphic corresponds to high-affinity type adsorption, which has a strong bond between adsorbent and adsorbate [27].

Batch Adsorption Experiment

The duration of reaction time in the adsorption process is a critical factor. Belonging the diffusion and adhesion of adsorbate molecules in the adsorbent surface area will be affected [28]. The optimal duration of contact time was determined by conducting experiments on the adsorption process, shown in the Figure 3 (a). As per the AAS analysis (15 to 120 minutes), variation delivers the optimum contact time on 30 minutes reaction to reach the presence absorption of 81.3% and the equilibrium adsorption capacity (q_e) uptake 8.13 mg/g for initial concentration of Cu^{2+} 10 mg/L on SBAC-1activation process. Besides that, correlation between % absorption and absorption capacity shown in Figure 3(b), which is derived from the quantity of adsorbate that may build up on the adsorbent's surface and expressed as a percentage. After the effect reaches the equilibrium point, the active site is switched off, and the adsorbent starts the desorption process and no longer takes the adsorbates [29].

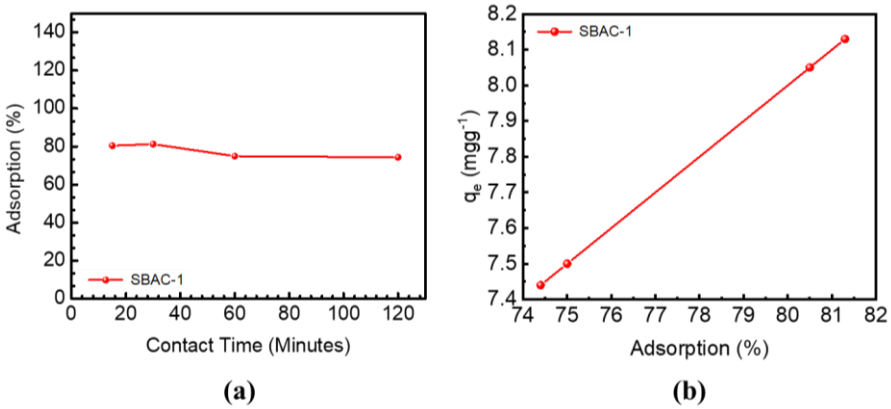

Figure 3. The impact of contact time on absorption in the presence (a) and correlation of percent absorption with absorption capacity (q_e) for base activation (b).

The starting point of concentration of metal ions in a liquid solution significantly influences metal adsorption [30]. The result of capacity adsorption also obtained by AAS analysis using (2.5 to 15 mg/L) variation brings about an optimum initial concentration of 5 mg/L with 82.2 % absorption (Figure 4(a)). It reaches 11.06 mg/g, the absorption capacity on 15 mg/L initial concentration on SBAC-1 activation process (Figure 4(b)). The distribution of metal ions on the adsorbent surface has become more competitive due to high temperatures [31].

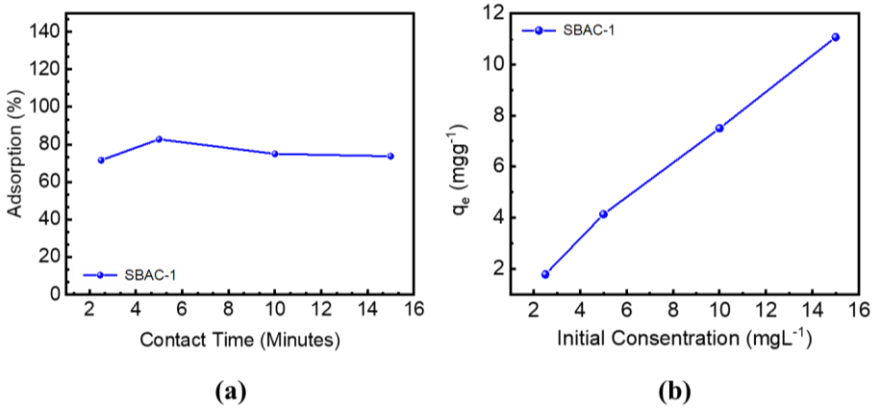

Figure 4. The impact of initial concentration with the presence absorption (a) and correlation of initial concentration with absorption capacity (mg/g) (b).

Determination of Experimental Model

Table 3. The experimental and theoretical values of q_e comparison.

No	C_o (mg/L)	C_e (mg/L)	Theoretical Value of qe (mg/g)	q_e (mg/g) Isotherm Equation	
				Freundlich	Langmuir
1.	2.5	0.71	1.79	1.88	3.17
2.	5	0.86	4.14	3.93	3.18
3.	10	2.5	7.5	7.06	3.19
4.	15	3.94	11.06	11.64	3.2

The adsorption capacity results obtained from the initial concentration (C_o) parameters were compared with the final concentration (C_e) value by the batch adsorption processes to prove the results of adsorption capacity (q_e) theoretically compared with actual experimental results using two types of isotherms, the findings are presented in Table 3. The theoretical value was obtained from AAS analysis carried out in BRIN's laboratory from research on copper metal ions in water analysed at a wavelength of 324.8 nm by the Badan Standarisasi Nasional Indonesia SNI 6989-84-2019 which has been issued with a SK number 513/KEP/BSN/11/2019. From various variations in initial concentration, the absorption capacity value closer to the theoretical is obtained using the Freundlich isotherm, compared to the Langmuir isotherm. For the Freundlich isotherm, the maximum adsorption capacity attained by the greatest starting concentration (15 mg/L) is 11.64 mg/g, with the outcome approximating the predicted value of 11.06 mg/g. The second highest value was followed by 10, 5, and 2.5 mg/L initial concentration value, that each valsue also approaching the theoretical value. However, the adsorption capacity from isotherm Langmuir result has a similar value each other ±3mg/g that have smaller value than Freunlich isotherm. So, this shows that The Freundlich isotherm is more successful than the Langmuir isotherm, as seen by acquiring a more prominent adsorption capacity figure close to the theoretical value.

The Langmuir Isotherm, the equilibrium of the interaction system between the absorbent and the adsorbate, where adsorption on the adsorbate is limited by one molecular layer (monolayer) when the relative pressure is reached. Meanwhile, Freundlich isotherm occurs due to physical interaction between the adsorbate and the adsorbent surface. The selection of the isotherm model is determined through the line equation obtained from the plot of each data, and the determination of the adsorption mechanism can be known.

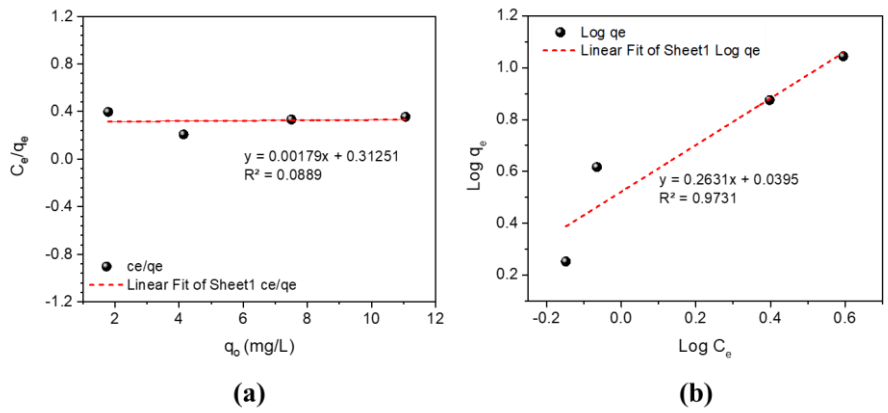

Figure 5. Linearization of Isotherm Langmuir (a) and linearization of Isotherm Freundlich (b).

Figure 5 (a) shows the adsorption fitting results obtained from the initial concentration parameters by linear regression from experiment data Cu^{2+} concentration using Langmuir model, also the regression coefficient value (R^2) was determined to be 0.0889. Using equation 5 and 6, the estimated values for q_{max} and K_L achieves 11.25 mg/g and 0.028 L/mg, respectively. While, in Figure 5 (b), the adsorption results were analysed using the Freundlich Adsorption isotherm, with log q_e plotted against log C_e and a least square fit method applied. The regression coefficient value (R^2) reached 0.9731. The heterogeneity factor of adsorption, represented by the reciprocal of n, was calculated to be 3.8. In contrast, the Freundlich constant characteristic (K_F), which can be interpreted as the maximum adsorption capacity, was obtained at 2.483. Based on the values of R^2, n, and KF obtained from the data presented in Figure 5 by equation 4, it can be inferred that among the two adsorption isotherm models discussed, the Freundlich isotherm model is the most suitable choice for depicting the adsorption process in this research.

This result was evidenced by the R^2 value of 0.9731, which is closer to 1 than the R^2 value from the Langmuir isotherm model. Hence, it is indicated that this study's adsorption mechanism was valid in multilayer adsorption processes [32]. The adsorption can be interpreted as adsorption that occurs in several layers of adsorbent with bonds that are not strong, which is assumed to be a heterogeneous adsorption site [33]. Multilayer adsorption is applicable, meaning that it considers the formation of multiple layers of adsorbate molecules on the surface of the adsorbent [34]. It's essential to note that Freundlich adsorption is often used to describe physical adsorption, where molecules adhere to a surface through van der Waals forces, hydrogen bonding, like thus, the adsorbent and adsorbate have a weaker connection. Until the adsorption process occurs in several layers, this permits the adsorbate to move freely [35-36].

Activated carbon which has pores with a high surface area will come into direct contact with the metal solution for the adsorption process. But the highlight is that multilayer adsorption could occur in combined first monolayer through interaction between Cu and SBAC surface. The molecules will be stuck into the active site on activated carbon through physical forces, van der waals, electrostatic interaction, also chemical interaction with ion exchange or formation of chemical bonds. The second layer as multilayer adsorption, the Cu ions remaining in the solution will continue to interact with SBAC to form the additional adsorption layer. Cu ions here will pile on the first monolayer which has formed or penetrated into the pores of the SBAC to form a deeper adsorption layer. The adsorption process continues until it reaches equilibrium where the rate of metal ion adsorption is the same as the desorption rate. Thus, the number of metal ions adsorbed on the activated carbon surface remains constant. From the adsorption-desorption curve in Figure 2, the final mechanism of adsorption processes was found in high-affinity adsorption with an indication of physiochemical adsorption.

Removal Percentage

Overall, the process activation variations from SBAC-1, SBAC-2, and SBAC-3 provide the percentage removal, showing the decrease of Cu^{2+} ions in the liquid samples. All of these factors are reflected in the percentage of removal indicated in Table 4. The base activated carbon (SBAC-1) had the best performance regarding %removal and adsorption capacity with a contact time of 30 minutes from the data of the contact time effect that has been conducted. In the sense that the SBAC-1 has been cleaned up from impurities better than SBAC-2, indicated by increasing the adsorption capacity. There is correlation of the good result of SBAC-1 sample with surface structure analysis. In Table 2, SBAC-1 shows a larger surface area provides more sites for the molecules of the target substance to adsorb, while a

greater pore volume facilitates the easy capture of these molecules. Together, these factors lead to a higher removal percentage which shows in Tabel 4.

Table 4. Percentage Removal of AC

Sample Name	C_0 (mg/L)	C_e (mg/L)	%Removal
SBAC – 1	10	2.5	75
SBAC – 2	10	2.98	70.2
SBAC – 3	10	5.03	49.7

CONCLUSIONS

SBAC was synthesized through a carbonization process with variations in activation, chemical with base (SBAC-1), chemical with acid (SBAC-2), and physics as Cu removal. The success of SBAC was proven through FTIR analysis with the appearance of peaks C=O, and C-O. visible differences in the appearance of the O-H group in samples SBAC-1 and SBAC-3 at 3200-2800 cm^{-1} and 3700-3200 cm^{-1}, whereas in that wavelength range, no single peak was visible in SBAC-2, due to the compound HCl acid cannot absorb the carbonate compound in sugarcane bagasse. Another characterization is proven through BET with prominent surface area was occupied by SBAC-1, reaching 458.607 m^2/g, followed by SBAC-3 and SBAC-2, 25.711 m^2/g and 20.408 m^2/g sequentially. The Cu removal test was carried out using test solution media from $CuSO_4$ for 2.5, 5, 10, and 15 ppm and 15, 30, 60, and 120 minutes for the length of contact time with SBAC-1 samples as the biggest surface area, and had q_{max} = 8.13 mg/g with successful removal achieved 75%, the highest adsorption capacity. The linear regression methods brings about the adsorption mechanism as physichemical & multilayer adsorption, with first monolayer and second multilayer adsorption with percent removal of Cu^{2+} at 81.3% at 30 minutes optimum time and optimum initial concentration of 5 mg/L with 82.2 % absorption on SBAC-1. The determination of Freundlich as the isotherm model is the most suitable mechanism of absorption for all process variations and produces an R^2 value of 0.9731 for the SBAC-1 sample.

ACKNOWLEDGMENTS

The analysis work is supported by PT. Pertamina Persero, and Laboratorium of Chemical Engineering Universitas Pertamina.

REFERENCES

1 Amanah, N. L., Djafar, E., Widharyanti, I. D., & Nugroho, A. 2023. Inhibition efficiency of water-soluble chitosan inhibitor from fish scales waste on low carbon steel SS400 in NaCl solution. *AIP Conference Proceedings*, 2743(1), 20010.

2 Amanah, N. L., Widharyanti, I. D., & Nugroho, A. 2021. Synthesis of water-soluble chitosan inhibitor from shrimp shells and its corrosion rate on mild steel in acidic solution. *Journal of Physics: Theories and Applications*, 5(1), 9–17.

3 Velusamy, S., Roy, A., Sundaram, S., & Kumar Mallick, T. 2021. A Review on Heavy Metal Ions and Containing Dyes Removal Through Graphene Oxide-Based Adsorption Strategies for Textile Wastewater Treatment. *The Chemical Record*, 21(7), 1570–1610.

4 Rajoria, S., Vashishtha, M., & Sangal, V. K. 2022. Treatment of electroplating industry wastewater: a review on the various techniques. *Environmental Science and Pollution Research International*, 29(48), 72196–72246.

5 Chaemiso, T. D. 2019. Removal Methods of Heavy Metals from Laboratory Wastewater. *Journal of Natural Sciences Research*.

6 Nugroho, A., Amanah, N. L., & Firdaus, R. G. 2022. Adsorption study of mango peel activated carbon as iron removal for batik waste industry. *Jurnal Rekayasa Proses*, 16(1), 19–24.
7 Amuda, O. S., Giwa, A. A., & Bello, I. A. 2007. Removal of heavy metal from industrial wastewater using modified activated coconut shell carbon. *Biochemical Engineering Journal*, 36(2), 174–181.
8 Kadirvelu, K., Kavipriya, M., Karthika, C., Radhika, M., Vennilamani, N., & Pattabhi, S. 2003. Utilization of various agricultural wastes for activated carbon preparation and application for the removal of dyes and metal ions from aqueous solutions. *Bioresource Technology*, 87(1), 129–132.
9 Masoud, M. S., El-Saraf, W. M., Abdel - Halim, A. M., Ali, A. E., Mohamed, E. A., & Hasan, H. M. I. 2016. Rice husk and activated carbon for waste water treatment of El-Mex Bay, Alexandria Coast, Egypt. *Arabian Journal of Chemistry*, 9, S1590–S1596.
10 Zakir, M., Kasim, H., Raya, I., Lamba, Y., Nuratisah, & Belen Jorge, A. 2019. Performance of Candlenut Shell (Alleuretus moluccana) Based Supercapacitor Electrode with Acid Electrolytes and Their Salts. *IOP Conference Series: Materials Science and Engineering*, 619(1), 12042.
11 Dias, M. O. S., Ensinas, A. V, Nebra, S. A., Maciel Filho, R., Rossell, C. E. V, & Maciel, M. R. W. 2009. Production of bioethanol and other bio-based materials from sugarcane bagasse: Integration to conventional bioethanol production process. *Chemical Engineering Research and Design*, 87(9), 1206–1216.
12 Chandel, A. K., Albarelli, J. Q., Santos, D. T., Chundawat, S. P., Puri, M., & Meireles, M. A. A. 2019. Comparative analysis of key technologies for cellulosic ethanol production from Brazilian sugarcane bagasse at a commercial scale. *Biofuels, Bioproducts and Biorefining*, 13(4), 994–1014.
13 Ghosh, A., Chakravorty, D., Rahaman, M., & Bose, S. 2019. Efficiency of Mango Peel Derived Activated Carbon Prepared via Different Routes as Adsorbent for Rhodamine B BT - Waste Water Recycling and Management. In S. K. Ghosh (Ed.) (pp. 111–122). Singapore: Springer Singapore.
14 Nasti, A. N. De, Siburian, K. Y., Sembiring, A. D., Kristianto, H., Susanti, R. F., Oktaviano, H. S., & Nugroho, A. 2023. Carbon composite of NiO hydrothermal impregnation from sugarcane bagasse and its electrochemical properties. *Jurnal Rekayasa Proses; Vol 17, No 2 (2023)DO - 10.22146/Jrekpros.88210* .
15 Agarwal, A. K., Kadu, M. S., Pandhurnekar, C. P., & Muthreja, I. L. 2013. Removal of Nickel (II) ions from aqueous solution using thermal power plant fly ash as a low cost adsorbent: Adsorption isotherm and kinetics study. *International Journal of Environmental Protection*, 3(3), 33.
16 Heidarinejad, Z., Dehghani, M. H., Heidari, M., Javedan, G., Ali, I., & Sillanpää, M. 2020. Methods for preparation and activation of activated carbon: a review. *Environmental Chemistry Letters*, 18(2), 393–415.
17 Lillo-Ródenas, M. A., Cazorla-Amorós, D., & Linares-Solano, A. 2003. Understanding chemical reactions between carbons and NaOH and KOH: An insight into the chemical activation mechanism. *Carbon*, 41(2), 267–275.
18 Kwaghger, A., & Ibrahim, J. S. 2013. Optimization of conditions for the preparation of activated carbon from mango nuts using HCl. *American Journal of Engineering Research*, 2(7), 74–85.
19 Hassan, A. F., Abdel-Mohsen, A. M., & Fouda, M. M. G. 2014. Comparative study of calcium alginate, activated carbon, and their composite beads on methylene blue adsorption. *Carbohydrate Polymers*, 102, 192–198.
20 Kim, D., Lee, K., & Park, K. Y. 2016. Upgrading the characteristics of biochar from cellulose, lignin, and xylan for solid biofuel production from biomass by hydrothermal carbonization. *Journal of Industrial and Engineering Chemistry*, 42, 95–100.

21 Guo, Y., Tan, C., Sun, J., Li, W., Zhang, J., & Zhao, C. 2020. Porous activated carbons derived from waste sugarcane bagasse for CO2 adsorption. *Chemical Engineering Journal*, 381, 122736.

22 Kiełbasa, K., Bayar, Ş., Varol, E. A., Sreńscek-Nazzal, J., Bosacka, M., Miądlicki, P., … Michalkiewicz, B. 2022. Carbon Dioxide Adsorption over Activated Carbons Produced from Molasses Using H2SO4, H3PO4, HCl, NaOH, and KOH as Activating Agents. *Molecules*.

23 Sricharoenchaikul, V., Pechyen, C., Aht-ong, D., & Atong, D. 2008. Preparation and Characterization of Activated Carbon from the Pyrolysis of Physic Nut (Jatropha curcas L.) Waste. *Energy & Fuels*, 22(1), 31–37.

24 Beyan, S. M., Prabhu, S. V., Ambio, T. A., & Gomadurai, C. 2022. A Statistical Modeling and Optimization for Cr(VI) Adsorption from Aqueous Media via Teff Straw-Based Activated Carbon: Isotherm, Kinetics, and Thermodynamic Studies. *Adsorption Science & Technology*, 2022, 7998069.

25 Cheng, L., Jiang, Y., Qi, S.-C., Liu, W., Shan, S.-F., Tan, P., … Sun, L.-B. 2018. Controllable Adsorption of CO2 on Smart Adsorbents: An Interplay between Amines and Photoresponsive Molecules. *Chemistry of Materials*, 30(10), 3429–3437.

26 Tan, Y. H., Davis, J. A., Fujikawa, K., Ganesh, N. V., Demchenko, A. V, & Stine, K. J. 2012. Surface area and pore size characteristics of nanoporous gold subjected to thermal, mechanical, or surface modification studied using gas adsorption isotherms, cyclic voltammetry, thermogravimetric analysis, and scanning electron microscopy. *Journal of Materials Chemistry*, 22(14), 6733–6745.

27 Naderi, M. 2015. Chapter Fourteen - Surface Area: Brunauer–Emmett–Teller (BET). In S. B. T.-P. in F. and S. Tarleton (Ed.) (pp. 585–608). Oxford: Academic Press.

28 Wang, S., Lu, L., Wu, D., Lu, X., Cao, W., Yang, T., & Zhu, Y. 2016. Molecular Simulation Study of the Adsorption and Diffusion of a Mixture of CO2/CH4 in Activated Carbon: Effect of Textural Properties and Surface Chemistry. *Journal of Chemical & Engineering Data*, 61(12), 4139–4147.

29 Tan, P., Bao, Y.-F., Liu, D.-H., Liu, X.-Q., & Sun, L.-B. 2023. Photomodulation on Active Sites of Adsorbents: Controllable Adsorption Processes with Improved Efficiency. *Chemistry – A European Journal*, n/a(n/a), e202300553.

30 Sari, A. P., Rhamadani, F. A., Amanah, N. L., & Nugroho, A. 2022. Study of Efficiency and Reaction Rates Dechlorination of Nata De Coco Wastewater Using Sodium Thiosulfate. *Journal of Emerging Supply Chain, Clean Energy, and Process Engineering* , 1(2 SE-ARTICLES), 107–116.

31 Wasewar, K. L. 2010. Adsorption of metals onto tea factory waste: a review. *International Journal of Research*, 3, 303–322

32 Kalam, S., Abu-Khamsin, S. A., Kamal, M. S., & Patil, S. 2021. Surfactant Adsorption Isotherms: A Review. *ACS Omega*, 6(48), 32342–32348.

33 Ragadhita, R., & Nandiyanto, A. B. D. (n.d.). How to Calculate Adsorption Isotherms of Particles Using Two-Parameter Monolayer Adsorption Models and Equations. *Indonesian Journal of Science and Technology; Vol 6, No 1 (2021): IJOST: April 2021DO - 10.17509/Ijost.V6i1.32354* .

34 Mohammed, I., Afagwu, C. C., Adjei, S., Kadafur, I. B., Jamal, M. S., & Awotunde, A. A. 2020. A review on polymer, gas, surfactant and nanoparticle adsorption modeling in porous media. *Oil Gas Sci. Technol. – Rev. IFP Energies Nouvelles*, 75.

35 Raji, Z., Karim, A., Karam, A., & Khalloufi, S. 2023. Adsorption of Heavy Metals: Mechanisms, Kinetics, and Applications of Various Adsorbents in Wastewater Remediation—A Review. *Waste*.

36 Sobolev, K. V, Magomedov, K. E., Shilov, N. R., Rodionova, V. V, & Omelyanchik, A. S. 2023. Adsorption of Copper Ions on the Surface of Multilayer Ti3C2Tx MXenes with Mixed Functionalization. *Nanobiotechnology Reports*, 18(1), S84–S89.